Journal of Robotics and Control (JRC)
Volume 5, Issue 6, 2024
ISSN: 2715-5072, DOI: 10.18196/jrc.v5i6.23800

Performance Analysis of PID and SMC Control Algorithms on AUV under the Influence of Internal Solitary Wave in the Bali Deep Sea

Kadek Dwi Wahyuadnyana [1], Katherin Indriawati [2*], Purwadi Agus Darwito [3], Ardyas Nur Aufa [4], Hilton Tnunay [5]
[1, 2, 3] Department of Engineering Physics, Intitut Teknologi Sepuluh Nopember (ITS), Surabaya 60111, Indonesia
[1, 4, 5] Beehive Intelligent Robotics Laboratory (BIRL), Beehive Drones, Yogyakarta 55582, Indonesia
[5] School of Electrical Engineering and Informatics, Institut Teknologi Bandung (ITB), Bandung 40132, Indonesia
Email: [1] dwiwahyuadnyana@gmail.com, [2] katherin@ep.its.ac.id, [3] padarwito@gmail.com, [4] ardyasnuraufa@gmail.com, [5] hilton.tnunay@itb.ac.id
*Corresponding Author

***Abstract*—Autonomous Underwater Vehicles (AUVs) play a crucial role in deep-sea exploration, but their stability is often compromised by Internal Solitary Waves (ISWs) and nonlinear disturbances in stratified waters. This study aims to evaluate the performance of two control algorithms, Proportional-Integral-Derivative (PID) and Sliding Mode Control (SMC), in mitigating ISW effects on AUV trajectory tracking. Simulations were conducted in Simulink (MATLAB), modeling AUV dynamics under ISW disturbances with intensities ranging from 0% to 100%. The results reveal that both PID and SMC algorithms experience significant performance degradation as ISW intensity increases, with Root Mean Square Error (RMSE) values rising exponentially between 50% and 75% disturbance levels. While SMC offers better resilience to nonlinear disturbances than PID, neither algorithm fully compensates for high ISW intensities. These findings highlight the limitations of conventional control strategies and underscore the need for more robust, adaptive algorithms for reliable deep-sea AUV operations. Future work will explore Nonlinear Model Predictive Control (NMPC) for improved stability in complex marine environments.**

***Keywords*—Autonomous Underwater Vehicle (AUV); Internal Solitary Waves (ISW); PID; SMC.**

I. INTRODUCTION

Recently, there has been a growing emphasis on the use of Autonomous Underwater Vehicles (AUVs) in deep-sea exploration by researchers [1][2], government agencies [3][4], and private industries [5][6]. AUVs are integral to advancing our understanding of ocean conditions and promoting sustainable marine resource utilization. In Indonesia, renowned for its rich marine biodiversity and valuable underwater mineral deposits, deploying AUVs is crucial to explore these resources effectively. However, one of the most significant obstacles facing underwater exploration is the presence of Internal Solitary Waves (ISW) [7][8][9][10][11][12].

Regarding the impact of ISW on underwater objects, a study by [13] has analyzed to evaluate the effects of the interaction between ISWs and a fixed submerged body. The research indicates that the hydrodynamic performance of the submerged object is significantly influenced when the object is located near the wave's central region. Furthermore, the magnitude of the force exerted on the object is primarily determined by the wave's amplitude. However, this study only focuses on the effects of ISWs on a stationary underwater object and does not account for moving objects, such as AUVs. This omission leaves a gap in understanding how ISWs would affect AUVs, which experience additional dynamics due to movement. Further investigation is required into how ISWs may alter trajectory, control, and stability in such mobile systems.

ISW, characterized by sudden shifts in underwater pressure and currents as external disturbance forces, can severely disrupt the stability of AUVs and the accuracy of the data they collect. These disturbances challenge collecting reliable marine data and equipment safety, as ISWs can affect navigation and control systems. This paper addresses how AUV control systems, specifically through advanced algorithms, can mitigate the effects of ISW during missions.

Focusing on the third core function of AUVs—control, particularly for regulating movement under dynamic conditions—this study aims to explore the effectiveness of control algorithms in enhancing AUV stability in the presence of ISW disturbances. This issue is critical for ensuring the success of missions in Indonesia's underwater environments, which are resource-rich and highly complex. Through precise control mechanisms, AUVs can continue to perform accurate mapping, data collection, and exploration, even in areas significantly impacted by ISW disturbance.

Traditional control algorithms for AUVs can be categorized into linear and nonlinear types. Linear algorithms, such as Proportional-Integral-Derivative (PID) controllers [14][15][16][17], and Linear Quadratic Regulators (LQR) [18][19][20], are popular for their simplicity but are less effective under nonlinear conditions like those caused by ISW. Nonlinear algorithms, such as Sliding Mode Control (SMC) [21][22] and Backstepping controllers [23][24] offer more robust performance in complex underwater environments but rely heavily on accurate modeling, which is challenging in unpredictable marine conditions.

The PID controller from other studies introduced by [25] is employed for trajectory tracking missions of AUVs under various underwater disturbance conditions. This controller

plays a crucial role in maintaining the desired path of the AUV despite challenges such as currents, waves, and other environmental factors that can disrupt its course. In addition, several studies employ the LQR control algorithm, as proposed by [20], which aims to minimize the quadratic cost function associated with the system state and control signal, allowing for efficient and precise control in meeting system objectives. However, this algorithm relies on a linear-based model. The challenge is that AUV models and their environments are often nonlinear [26][27], making this control algorithm potentially less applicable under certain conditions. Furthermore, a nonlinear model-based control algorithm, specifically the SMC algorithm, was proposed by [28] and [29] to achieve robust AUV performance during trajectory tracking. This algorithm employs the concept of a sliding surface, which makes the system dynamics invariant to uncertainties and disturbances once the surface is reached.

However, SMC relies on the existing system model [30]. If this model is inaccurate or fails to capture all relevant nonlinear dynamics, the control performance may be compromised, leading to the system not achieving the desired performance. Another nonlinear control algorithm is the Backstepping controller, as proposed by [31][32][33]. It is designed for nonlinear systems using a layered approach, where control functions are developed incrementally to leverage the system's nonlinear dynamics. However, the practical implementation of the Backstepping controller requires extensive tuning and testing to achieve the desired performance due to challenges with external disturbances and model uncertainty [34][35][36].

Although various studies have explored linear and nonlinear control algorithms for AUVs, none have specifically examined deep-sea conditions, particularly the impact of ISWs on the AUV's stability. Most research depends on current and wave data derived from laboratory-based assumptions. In deeper sea exploration, the presence of ISW is unavoidable and can disrupt underwater missions for AUVs. For instance, research by [37] and [38] has indicated that ISW contributed to the April 2021 accident involving the Indonesian military submarine KRI Nanggala 402 in the deep sea of Bali. This highlights the necessity of considering ISW in deep-sea exploration. Therefore, this paper's contributions aim to investigate and assess the impact of ISW on AUV stability during deep-sea exploration using two conventional control algorithms: PID and SMC. The key objective of this study is to provide a thorough understanding of how ISW affects AUV stability, which will provide valuable information for the development of future control algorithms that will be more efficient and effective in maintaining AUV stability in the face of ISW disturbances during deep-sea exploration.

II. RESEARCH METHODOLOGY

The flowchart in Fig. 1 illustrates the research methodology in this study. It details the sequential steps taken to evaluate the performance of PID and SMC control algorithms on an AUV under the influence of ISW. Each step, from defining research objectives to analyzing results, is structured to comprehensively compare the control algorithms' effectiveness in managing ISW disturbances. This systematic approach ensures accurate performance assessment, providing insights into potential improvements for underwater vehicle control in complex marine environments.

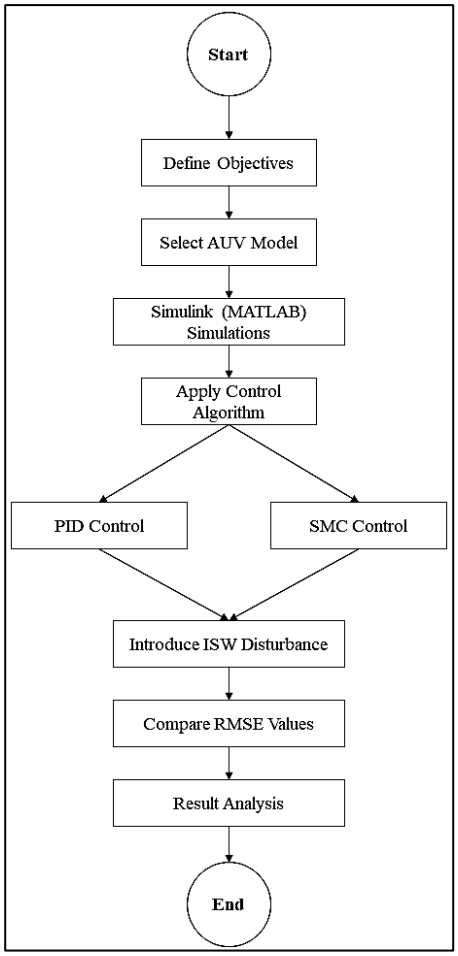

Fig. 1. The research methodology flowchart

The research methodology begins by defining the objectives, which focus on evaluating the performance of PID and SMC control algorithms in stabilizing an AUV under ISW disturbances. This step sets the research direction to assess how each control method handles nonlinear disturbances in deep-sea environments.

Next, the AUV model is selected, incorporating its dynamic and kinematic properties to simulate realistic underwater behavior. This ensures that the simulations reflect actual operating conditions, which is crucial for accurately evaluating the control algorithm's performance.

The Simulink (MATLAB) simulations are then conducted to apply the PID and SMC control algorithms separately. These algorithms guide the AUV along a predefined trajectory while managing disturbances. Afterward, ISW disturbances are introduced at varying intensities (0% to 100%) to test the algorithms' effectiveness in mitigating the impact of these forces.

The study proceeds by comparing the PID and SMC Root Mean Square Error (RMSE) values, which quantify the AUV's deviation from its intended trajectory under each control algorithm. This step provides a clear measure of

performance, highlighting the strengths and limitations of each approach.

Finally, the methodology concludes with a results analysis, where the findings are discussed, emphasizing the need for more advanced control strategies.

III. AUV Dynamic and Kinematic Models

A. AUV Model Selection and Description

AUVs are typically classified into three types based on their morphology: torpedo-like [39], symmetrical cube-like [40][41], and biomimetic (imitate the forms of marine life) [42][43]. A study by [44], through numerical simulations, suggests that the symmetrical cube AUV is the best choice for exploration missions, which aligns with the focus of this research on exploration. In contrast, the torpedo model is more suited for military applications due to its hydrodynamic design, enabling higher speeds [39], while the biomimetic model has a complex design and faces control and stability challenges [42][43]. Since exploration does not require such speed and needs to be efficient, the cube-shaped AUV is more appropriate due to its ease of control in all directions, as its shape and thrusters on each side provide superior maneuverability and stability. Therefore, this paper focuses on the symmetrical cube AUV model.

The BlueROV2 is a commercial Remotely Operated Vehicle (ROV) from Blue Robotics [45][46], designed in a symmetrical cube shape, as shown in Fig. 2. It is well-regarded for its stability, agility, and excellent imaging capabilities. A key feature of BlueROV2 is its open-source platform, which enables researchers to modify and enhance the vehicle to meet specific research requirements. The ROV comes with a factory-installed remote control (RC) and a user interface that is ready to use. However, this paper does not require RC features. Instead, it uses the ROV model to apply and test various control algorithms studied in this paper. The BlueROV2 uses six thrusters to maneuver underwater, as shown in Fig. 3. Four of these thrusters are configured to control surge (u), sway (v), and yaw (r) movements, while the other two are dedicated to facilitating heave motion. This model does not account for roll (p) and pitch (q) movements [47].

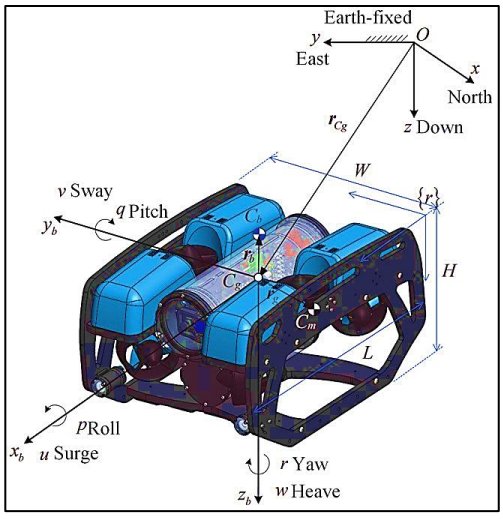

Fig. 2. AUV frame of reference

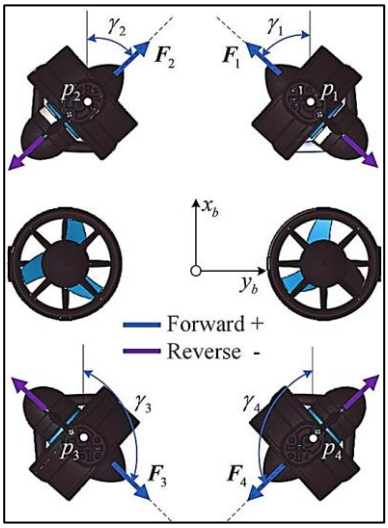

Fig. 3. AUV thruster configurations

A detailed understanding of the AUV's kinematic and dynamic models is essential to implementing autonomous control algorithms. Several studies, including those by [48][47][40], have described and validated the BlueROV2 kinematic and dynamic model. Furthermore, the authors adopt and adjust these models to fit the specific focus of the current study.

B. Dynamic Model of AUV

The ROV dynamics are described by differential equations relating to the vehicle's position and velocity. The reference position, denoted as $\boldsymbol{\eta} = [x \quad y \quad z \quad \phi \quad \theta \quad \psi]^T$, represents the vehicle's pose relative to a fixed global reference system. Here, x, y, and z denote the position as illustrated in Fig. 2, while ϕ, θ, and ψ represent the orientation following the right-hand rule. The velocity, denoted as $\boldsymbol{\nu} = [u \quad v \quad w \quad p \quad q \quad r]^T$, includes both linear and angular components relative to the ROV's body. In this context, u, v, and w represent the rates of translation and p, q, and r represent the rates of rotation.

The dynamic equations for underwater vehicles were initially developed by Fossen [49][50], and already studied and validated by [41][47][48]. This equation has been adapted to model the dynamics of the BlueROV2, with parameters customized for this specific vehicle. The Fossen equation is detailed in (1). The term $\boldsymbol{M}_{RB}$ is for the force and moment due to the acceleration of ROV rigid body mass and $\boldsymbol{M}_A$ is the water added mass around the ROV body, which are given in (2), and (3) respectively. Based on (2) and (3), m is the total mass of ROV, x_G, y_G, z_G are the position of the center of gravity. I_x, I_y, I_z are the moment inertia of each axis, and I_{ij} is the product of with respect to i, j plane that measures the imbalance of mass distribution, $\boldsymbol{X}_{\dot{u}}, \boldsymbol{Y}_{\dot{v}}, \boldsymbol{Z}_{\dot{w}}$ are the added mass in x, y, z direction due to translation in water, and $\boldsymbol{K}_{\dot{p}}, \boldsymbol{M}_{\dot{q}}, \boldsymbol{N}_{\dot{r}}$ are the increased inertia about x, y, z axis due to rotation in water. Coriolis force matrix also consists of rigid body ($\boldsymbol{C}_{RB}$) and the added mass ($\boldsymbol{C}_A$) which are given in (4), and (5) respectively. The term $\boldsymbol{D}$ is the hydrodynamic damping as given in (6), with $\boldsymbol{P} = \boldsymbol{X}_{u|u} + \boldsymbol{X}_u$, $\boldsymbol{Q} = \boldsymbol{Y}_{v|v} + \boldsymbol{Y}_v$, $\boldsymbol{R} = \boldsymbol{Z}_{w|w} + \boldsymbol{Z}_w$, $\boldsymbol{S} = \boldsymbol{K}_{p|p} + \boldsymbol{K}_p$, $\boldsymbol{T} = \boldsymbol{M}_{q|q} + \boldsymbol{M}_q$, $\boldsymbol{U} = \boldsymbol{N}_{r|r} + \boldsymbol{N}_r$. The term $\boldsymbol{g}(\eta)$ is the hydrostatic restoring forces

vector as given in (7), where $c(\cdot) = \cos(\cdot)$, $and\ s(\cdot) = \sin(\cdot)$. The term $\boldsymbol{\tau}$ is the propulsion forces vector as given in (8), to which the control algorithm will be applied in this term. And, the term $\boldsymbol{\tau}_{ext}$ is the external disturbances, in this case, ISW will be applied, which will be explained in the following section.

$$M_{RB}\dot{v} + C_{RB}(v)v + M_A\dot{v} + C_A(v_r)v_r + D(v_r)v_r + g(\eta) = \tau + \tau_{ext} \quad (1)$$

$$M_{RB} = \begin{bmatrix} m & 0 & 0 & 0 & mz_G & -my_G \\ 0 & m & 0 & -mz_G & 0 & mx_G \\ 0 & 0 & m & my_G & -mx_G & 0 \\ 0 & -mz_G & my_G & I_x & I_{xy} & I_{xz} \\ mz_G & 0 & -mx_G & I_{yx} & I_y & I_{yz} \\ -my_G & mx_G & 0 & I_{zx} & I_{zy} & I_z \end{bmatrix} \quad (2)$$

$$M_A = -\begin{bmatrix} X_{\dot{u}} & 0 & 0 & 0 & 0 & 0 \\ 0 & Y_{\dot{v}} & 0 & 0 & 0 & 0 \\ 0 & 0 & Z_{\dot{w}} & 0 & 0 & 0 \\ 0 & 0 & 0 & K_{\dot{p}} & 0 & 0 \\ 0 & 0 & 0 & 0 & M_{\dot{q}} & 0 \\ 0 & 0 & 0 & 0 & 0 & N_{\dot{r}} \end{bmatrix} \quad (3)$$

$$C_{RB} = \begin{bmatrix} 0 & 0 & 0 & 0 & mw & -mv \\ 0 & 0 & 0 & -mw & 0 & mu \\ 0 & 0 & 0 & mv & -mu & 0 \\ 0 & mw & -mv & 0 & I_z r & -I_y q \\ -mw & 0 & mu & -I_z r & 0 & I_x p \\ mv & -mu & 0 & I_y q & -I_x p & 0 \end{bmatrix} \quad (4)$$

$$C_A = \begin{bmatrix} 0 & 0 & 0 & 0 & -Z_{\dot{w}}w & Y_{\dot{v}}v \\ 0 & 0 & 0 & Z_{\dot{w}}w & 0 & -X_{\dot{u}}u \\ 0 & 0 & 0 & -Y_{\dot{v}}v & X_{\dot{u}}u & 0 \\ 0 & -Z_{\dot{w}}w & Y_{\dot{v}}v & 0 & -N_{\dot{r}}r & M_{\dot{q}}q \\ Z_{\dot{w}}w & 0 & -X_{\dot{u}}u & N_{\dot{r}}r & 0 & -K_{\dot{p}}p \\ -Y_{\dot{v}}v & X_{\dot{u}}u & 0 & -M_{\dot{q}}q & K_{\dot{p}}p & 0 \end{bmatrix} \quad (5)$$

$$D = -\begin{bmatrix} P & 0 & 0 & 0 & 0 & 0 \\ 0 & Q & 0 & 0 & 0 & 0 \\ 0 & 0 & R & 0 & 0 & 0 \\ 0 & 0 & 0 & S & 0 & 0 \\ 0 & 0 & 0 & 0 & T & 0 \\ 0 & 0 & 0 & 0 & 0 & U \end{bmatrix} \quad (6)$$

$$g(\eta) = \begin{bmatrix} (W-B)s\theta \\ -(W-B)c\theta \cdot s\phi \\ -(W-B)c\theta \cdot c\phi \\ (z_G W - z_B B)c\theta \cdot s\phi \\ (z_G W - z_B B)s\theta + (x_H W - x_B B)c\theta \cdot c\phi \\ -(x_G W - x_B B)c\theta \cdot c\phi \end{bmatrix} \quad (7)$$

$$\tau = [\tau_x \quad \tau_y \quad \tau_z \quad \tau_\phi \quad \tau_\theta \quad \tau_\psi]^T \quad (8)$$

C. Kinematic Model of AUV

Besides the dynamic model, the kinematic model is also essential for robot simulation. The kinematic model provides critical insights into how a robot moves by focusing on its motion without considering the forces and torques involved. This model is vital for calculating the positions and orientations of the robot's joints and links, enabling precise control and trajectory planning. Equation (9) presents the kinematic equation for the ROV, which describes the relationship between its velocity in the body frame and its position in the earth-fixed frame. Based on (9), $\boldsymbol{J(\eta)}$ consists of transformation to the body velocity in the inertial reference frame, as given in (10). Based on (10), $\vec{\boldsymbol{R}}$ is the transformation matrix of the linear velocity as given in (11), and $\vec{\boldsymbol{T}}$ is the transformation matrix of the angular velocity as given in (12), where $t(\cdot) = \tan(\cdot)$. This kinematic model of AUV is also has been studied and validated by [48][51][52].

$$\dot{\boldsymbol{\eta}} = \boldsymbol{J(\eta)\nu} \quad (9)$$

$$\boldsymbol{J(\eta)} = \begin{bmatrix} \vec{\boldsymbol{R}} & 0_{3x3} \\ 0_{3x3} & \vec{\boldsymbol{T}} \end{bmatrix} \quad (10)$$

$$\vec{\boldsymbol{R}} = \begin{bmatrix} c\psi.c\theta & -s\psi.c\phi + c\psi.s\theta.s\phi & s\psi.s\phi + c\psi.c\phi.s\theta \\ s\psi.c\theta & c\psi.c\phi + s\phi.s\theta.s\psi & -c\psi.s\phi + s\theta.s\psi.c\phi \\ -s\theta & c\theta.s\phi & c\theta.c\phi \end{bmatrix} \quad (11)$$

$$\vec{\boldsymbol{T}} = \begin{bmatrix} 1 & s\phi.t\theta & c\phi.t\theta \\ 0 & c\theta & -s\theta \\ 0 & s\phi/c\theta & c\phi/c\theta \end{bmatrix}, \theta \neq \pm\frac{\pi}{2} \quad (12)$$

IV. Internal Solitary Wave (ISW) Theory and Modeling

Sea waves are typically generated by winds blowing across the surface. While waves are often believed only to affect the surface area, they can also influence the underwater environment to a certain depth under specific conditions [53][54]. Ocean currents are generally described as the movement of water masses or particles from one region to another, primarily driven by surface wave activity [55]. However, as the ocean depth increases, the effect of surface waves diminishes, as depicted in Fig. 4.

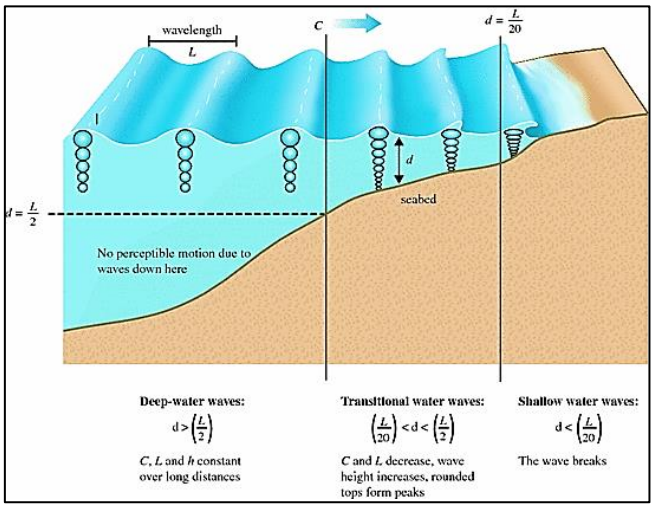

Fig. 4. Illustration of how the sea waves at the surface influence the underwater environment to a certain depth [53]

Beyond the visible surface waves, as given in Fig. 4, the ocean contains ISWs, which are not visible because they occur beneath the surface [56][57][58]. These waves form due to variations in temperature and salinity that cause unstable seawater density between different layers [59][60][61]. Indonesia's archipelagic structure significantly impacts its oceanic conditions. Variations in salt concentration caused by river estuaries and freshwater inflows lead to complex sea conditions [62]. Due to Pacific

currents, higher salinity in the eastern region affects underwater currents and waves [63]. Moreover, the diverse underwater topography, including large islands, straits, and valleys, influences flow patterns. For example, the narrow Strait of Malacca accelerates seawater movement, resulting in strong currents and large waves [64]. Thus, the potential for ISWs in Indonesia's deep waters is very high. To validate this theory, a study by [37] detected significant ISW activity near the KRI Nanggala-402 submarine wreck in April 2021. These ISWs originated in the Lombok Strait, moved northwest across the Bali Sea, passed the wreck site, and reached the continental shelf west of the Kangean Islands. Unlike earlier studies that found ISWs mainly north of Lombok Island, the April 2021 ISWs were mostly north of Bali Island, demonstrating notable temporal variation in their distribution. This indicates that ISWs are crucial, particularly for deep-sea exploration missions using technologies like AUVs, as they may affect system stability during operations.

To model these ISWs, the author of this paper needs to gather and examine several studies, including those by A and B. The model for ISW disturbances focuses on the current velocity generated by the ISWs. This velocity, occurring at specific ocean depths, is an unavoidable disturbance. Previous research has provided a mathematical framework for this, leading to the derivation of the equation for the current velocity caused by ISWs (v_{ISW}), as outlined in (13), where A is the ISW amplitude, g is the gravitational acceleration, h_1 and h_2 are the thickness of the upper and lower water layers, $\Delta p = \rho_1 - \rho_2$ is the relative layer density difference from the upper (ρ_1) and lower (ρ_2) layer density, and $\rho_0 = (\rho_1 + \rho_2)/2$. This model will be used to simulate disturbance effects on the AUV and will be applied to evaluate two control algorithms: PID and SMC. This v_{ISW} will act as a disturbance variable in analyzing how effectively these algorithms can manage such disturbances.

$$v_{ISW} = \left[\sqrt{\frac{g\Delta\rho h_1 h_2}{\rho_0(h_1+h_2)}}\right]\left[1 + A\frac{9}{2}\left(\frac{h_1 - h_2}{h_1 h_2}\right)\right] \quad (13)$$

A study by [37] observed significant ISW activity near the wreck site of the submarine KRI Nanggala-402 in April 2021. These waves originated in the Lombok Strait, traveled northwest across the Bali Sea, passed the wreck site, and reached the continental shelf west of the Kangean Islands. Unlike earlier findings that primarily located ISWs north of Lombok Island, the April 2021 ISWs were mainly north of Bali Island, indicating a notable temporal shift in their distribution. Up to three wave packets, each containing dozens of solitons with crests extending over 60 km and reaching 200 km in length, moved through the Bali Sea. According to (13), these ISWs traveled at an average speed of 2 m/s, peaking at 2.69 m/s in the basin and slowing to 0.71 m/s in shallow waters. On April 19, two days before the submarine incident, an ISW near the wreck site had an amplitude of 41 meters, with maximum horizontal and vertical velocities of 65 cm/s and 10 cm/s, respectively, as observed in satellite data. These ISWs were generated from the southward barotropic tidal trough, with two waves produced every 11.7 to 12.3 hours during the April tidal period.

The observations of ISW activity in the Bali Sea around the KRI Nanggala-402 wreck site underscore the significant impact these oceanic phenomena can have on underwater operations. ISWs are common in many marine environments worldwide, particularly in straits, continental shelves, and areas with complex bathymetry, like the Indonesian seas. These waves are characterized by their large amplitude and rapid propagation speed, which can create strong horizontal and vertical water movements. In real-world scenarios, ISWs can cause substantial disruptions to underwater vehicles, destabilizing AUVs and leading to potential mission failures by impairing navigation, sensor performance, and trajectory tracking. Given these risks, developing control algorithms is crucial as they provide resilience against the unpredictable and nonlinear forces generated by ISWs. By investigating the effects of ISWs on AUV stability, more adaptive and reliable control systems can be developed, ensuring better performance and reliability in the increasingly complex underwater environments where these vehicles operate.

V. CONTROL ALGORITHM DESIGNS

This paper examines two control algorithms: PID and SMC. These algorithms are selected based on their ease of implementation in the AUV dynamic system, especially the PID control algorithm. SMC is also chosen for its straightforward integration into the AUV dynamic system. Additionally, these algorithms represent two control approaches: PID for linear control and SMC for nonlinear control. Both control algorithms aim to minimize the error between the actual position and the reference during trajectory tracking. PID is widely used in industry and robotics due to its simplicity and effectiveness, while SMC is known for its robustness against external disturbances. This paper assesses the performance of each algorithm when applied to an AUV under ISW disturbances.

A. PID Controller

The PID control algorithm functions by combining three fundamental principles: Proportional (P), Integral (I), and Derivative (D) [65][66][67]. The (P) component adjusts the control output based on the current error, which is the difference between the desired setpoint and the actual position, making corrections proportional to this error [68]. After applying the proportional action, the (I) component accumulates past errors over time to address any residual steady-state error [69]. The (D) component also provides a control action that helps to dampen the response and enhance system stability by responding to how quickly the error changes [70].

In the context of the AUV model used in this paper, specifically the BlueROV2 model, several states are generated, including surge (u), sway (v), heave (w), and yaw (r). The other two states, roll (p) and pitch (q), are assumed to be stable and, therefore, set to zero. Consequently, the PID control algorithm must be applied to these four states—surge, sway, heave, and yaw—to manage their respective movements. This application of PID control is illustrated in Fig. 4.

According to Fig. 5, the BlueROV2 system is initially provided with a desired trajectory, represented by

(x_d, y_d, z_d, ψ_d). Simultaneously, BlueROV2 also sends its actual position, represented by (x, y, z, ψ). These values are compared to the reference trajectory to determine the error for each state: (e_x, e_y, e_z, e_ψ). This error data is then fed into the control algorithm, specifically the PID controller, which generates control laws in the form of u_x, u_y, u_z, u_ψ, for each surge, sway, heave, and yaw state. These control laws are then sent to the Thrusters Management System (TMS). These control laws are processed to determine the appropriate thrust for each of the six thrusters $(\tau_x, \tau_y, \tau_z, \tau_\phi, \tau_\theta, \tau_\psi)$ to follow the desired trajectory. At the same time, the BlueROV2 dynamic system is subjected to disturbances from the ISW Model, as given in (13). This continuous process allows BlueROV2 to follow the desired trajectory autonomously. Furthermore, the focus is on the design of the control laws. For the PID controller, the equations of the control laws for each state are provided in (14)-(17), where K_P, K_I, and K_D are the gain constants for each component of the PID control algorithm.

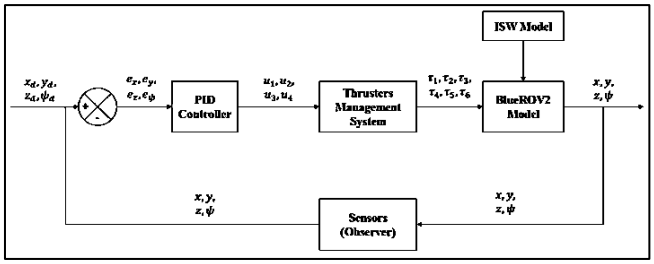

Fig. 5. Block diagram of the PID control algorithm for the BlueROV2 dynamic system

$$u_x = K_P e_x + K_I \int_0^t e_x \, dt + K_d \frac{d(e_x)}{dt} \tag{14}$$

$$u_y = K_P e_y + K_I \int_0^t e_y \, dt + K_d \frac{d(e_y)}{dt} \tag{15}$$

$$u_z = K_P e_z + K_I \int_0^t e_z \, dt + K_d \frac{d(e_z)}{dt} \tag{16}$$

$$u_\psi = K_P e_\psi + K_I \int_0^t e_\psi \, dt + K_d \frac{d(e_\psi)}{dt} \tag{17}$$

B. SMC Controller

Sliding Mode Control, or SMC, is a robust control technique to manage nonlinear systems with uncertainties and disturbances [71][72]. It defines a sliding surface in the state space, representing the desired system behavior. The control objective is to drive the system's states to this surface, or reaching phase, and keep them in the sliding phase, where the system dynamics become insensitive to certain disturbances and model uncertainties [73][74]. The primary objective of the SMC algorithm is to minimize error, much like other control algorithms. The critical difference lies in its unique method of minimizing that error. Therefore, the block diagram for the SMC algorithm applied to the BlueROV2 system, as used in this paper, can be seen in Fig. 5. Similar to Fig. 5, Fig. 6 illustrates the control process for the BlueROV2 system using the SMC control algorithm. The system receives the desired trajectory (x_d, y_d, z_d, ψ_d) and simultaneously reports its actual position (x, y, z, ψ). The difference between these values is calculated as errors (e_x, e_y, e_z, e_ψ) relative to the desired trajectory. These errors are processed by the SMC controller, which generates control laws u_x, u_y, u_z, u_ψ for each surge, sway, heave, and yaw movement. These control laws are sent to the TMS, which adjusts the thrust rates $(\tau_x, \tau_y, \tau_z, \tau_\phi, \tau_\theta, \tau_\psi)$ for the six thrusters to maintain the desired path. The BlueROV2 also deals with disturbances from the ISW model, as given in (13). This feedback loop continuously operates to autonomously guide BlueROV2 along its desired trajectory.

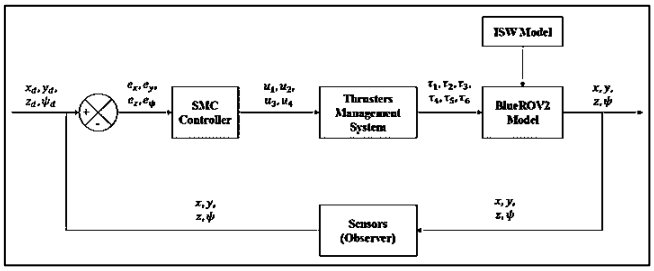

Fig. 6. Block diagram of the SMC control algorithm for the BlueROV2 dynamic system

In designing the SMC control laws for the BlueROV2 system, the dynamic equations provided in (1) are referenced. The main objective is to minimize the error between the desired trajectory and the actual position. Thus, the sliding surface is defined using the error in surge motion (e_x), as detailed in (18). To move the system into the reaching phase, $\dot{e}_x = 0$ is set, resulting in the control law for surge motion u_1 given by (19), where m_1 represents the rigid body mass in the surge direction, m_{a1} is the added mass in the surge direction, c_1 is the Coriolis term for surge, c_{a1} is the added mass Coriolis term for surge, d_1 is the damping term for surge, g_x is the restoring force in the surge direction, K is a positive gain and $sgn(\cdot)$ is the sign function as defined in (20). Similarly, control laws for other movements (sway, heave, and yaw) are obtained and are provided in (21)–(23).

$$e_x = \dot{x} - \dot{x}_d \tag{18}$$

$$u_x = (m_1 + m_{a1})\ddot{x}_d - c_1\dot{x} - c_{a1}v_r - d_1v_r - g_x + K_1 sgn(e_x) \tag{19}$$

$$sgn(e_x) = \begin{cases} 1, & e_x > 0 \\ 0, & e_x = 0 \end{cases} \tag{20}$$

$$u_y = (m_2 + m_{a2})\ddot{y}_d - c_1\dot{y} - c_{a1}v_r - d_1v_r - g_y + K_2 sgn(e_y) \tag{21}$$

$$u_z = (m_3 + m_{a3})\ddot{z}_d - c_1\dot{z} - c_{a1}v_r - d_1v_r - g_z + K_3 sgn(e_z) \tag{22}$$

$$u_\psi = (m_4 + m_{a4})\ddot{\psi}_d - c_1\dot{\psi} - c_{a1}v_r - d_1v_r - g_\psi + K_4 sgn(e_\psi) \tag{23}$$

VI. SIMULATION SETUP

A suitable vehicle or platform is required to support the simulations in this study to implement PID and SMC control algorithms and to model ISW disturbances to evaluate the

performance of these control algorithms under ISW disturbances. This paper utilizes an open-source simulator platform developed by [52], specifically designed for the BlueROV2. The platform is based on Simulink (MATLAB) and incorporates Fossen's equations, which include the kinematic and dynamic models of the BlueROV2, as detailed in (1)-(12). This platform accurately represents the real hardware conditions to a considerable extent, making it suitable for simulation processes before actual hardware implementation. The proposed platform's interface, as suggested by [52], is illustrated in Fig. 7, Fig. 8. Fig. 7 displays the Graphical User Interface (GUI) used to configure initial settings before running a simulation. This interface allows users to set parameters such as the initial speed and position of the BlueROV2. According to Fig. 7, several parameters are adjusted, as outlined in Table I to Table III. Fig. 8 illustrates the complete block diagram of the entire control system for the BlueROV2. This paper specifically focuses on incorporating the ISW disturbance model within the External Forces block within the Fig. 7. Based on Fig. 8, several parameters have been set to optimize the control algorithms and accurately represent the magnitude of the ISW disturbances, as detailed in Table II, where CO is the center of origin, COM is the center of mass, COB is the center of buoyancy, v_{ISW_X} is the ISW velocity in x direction, v_{ISW_Y} is the ISW velocity in y direction, and v_{ISW_Z} is the ISW velocity in z direction.

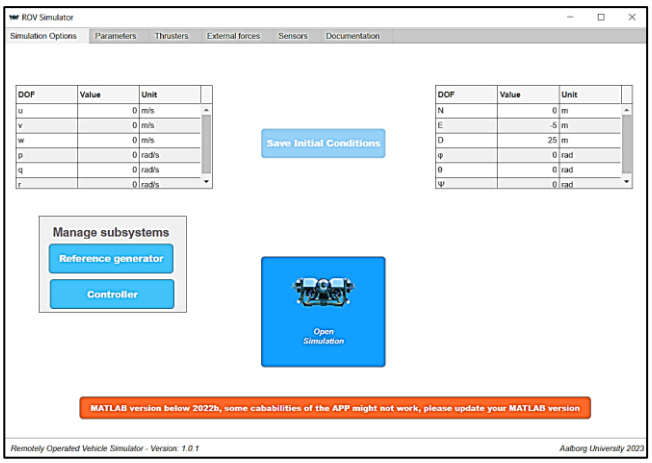

Fig. 7. The BlueROV2 simulator platform GUI proposed by [52]

TABLE I. THE INITIAL CONDITIONS OF BLUEROV2

Initial Positions		Initial Velocities	
x (N)	0 m	$\dot{x}$ (Surge-u)	0 m/s
y (E)	-5 m	$\dot{y}$ (Sway-v)	0 m/s
z (D)	25 m	$\dot{z}$ (Heave-w)	0 m/s
ψ	0 m	$\dot{\psi}$ (Yaw-r)	0 m/s

TABLE II. THE DIMENSSION AND HYDRODYNAMIC PARAMATERS OF BLUEROV2

Physical Dimenssions		
Parameters	**Value**	
The total mass of ROV	11 kg	
Volume of ROV	0.0135 m^3	
Height (L_H)	0.378 m	
Width (L_W)	0.575 m	
Length (L_L)	0.457 m	
Momen of Inertia		
Parameters	**Value**	
Momen of Inertia around x-axis (L_x)	0.26 kgm^2	
Momen of Inertia around y-axis (L_y)	0.23 kgm^2	
Momen of Inertia around z-axis (L_z)	0.37 kgm^2	
Weight and Buoyancy		
Parameters	**Value**	
Distance from CO to COM (x_g)	0 m	
Distance from CO to COM (y_g)	0 m	
Distance from CO to COM (z_g)	0 m	
Distance from CO to COB (x_b)	0 m	
Distance from CO to COB (y_b)	0 m	
Distance from CO to COB (z_b)	-0.01 m	
Linear Damping		
Parameters	**Value**	
When in Surge (X_u)	13.7 Ns/m	
When in Sway (Y_v)	0 Ns/m	
When in Heave (Z_w)	33 Ns/m	
When in Roll (K_p)	0 Ns/rad	
When in Pitch (M_q)	0.8 Ns/rad	
When in Yaw (N_r)	0 Ns/rad	
Quadratic Damping		
Parameters	**Value**	
When in Surge ($X_{u\|u}$)	141 Ns^2/m^2	
When in Sway ($Y_{v\|v}$)	217 Ns^2/m^2	
When in Heave ($Z_{w\|w}$)	190 Ns^2/m^2	
When in Roll ($K_{p\|p}$)	1.192 Ns^2/rad^2	
When in Pitch ($M_{q\|q}$)	0.47 Ns^2/rad^2	
When in Yaw ($N_{r\|r}$)	1.5 Ns^2/rad^2	
The Added Mass		
Parameters	**Value**	
When in Surge ($X_{\dot{u}}$)	6.516 kg	
When in Sway ($Y_{\dot{v}}$)	7.299 kg	
When in Heave ($Z_{\dot{w}}$)	19.15 kg	
When in Roll ($K_{\dot{p}}$)	0.1904 kg	
When in Pitch ($M_{\dot{q}}$)	0.1382 kg	
When in Yaw ($N_{\dot{r}}$)	0.227 kg	
The External Disturbance by the Tether		
Parameters	**Value**	
Length (L_{tet})	35 m	
Mass (m_{tet})	0.043 kg/m	
Diameter (d_{tet})	0.0075 m	
Youngs Modulus (E_{tet})	6.437×10^{10} N/m^2	
Normal Drag (Cn_{tet})	1.2	
Tangential Drag (Ct_{tet})	0.01	
Inertial Damping (Ci_{tet})	0 Ns/m	
The External Disturbance by the ISW in Bali Deep Sea		
Velocity	**Max**	**Min**
v_{ISW_X}	2.69 m/s	0.71 m/s
v_{ISW_Y}	0	0
v_{ISW_Z}	0	0

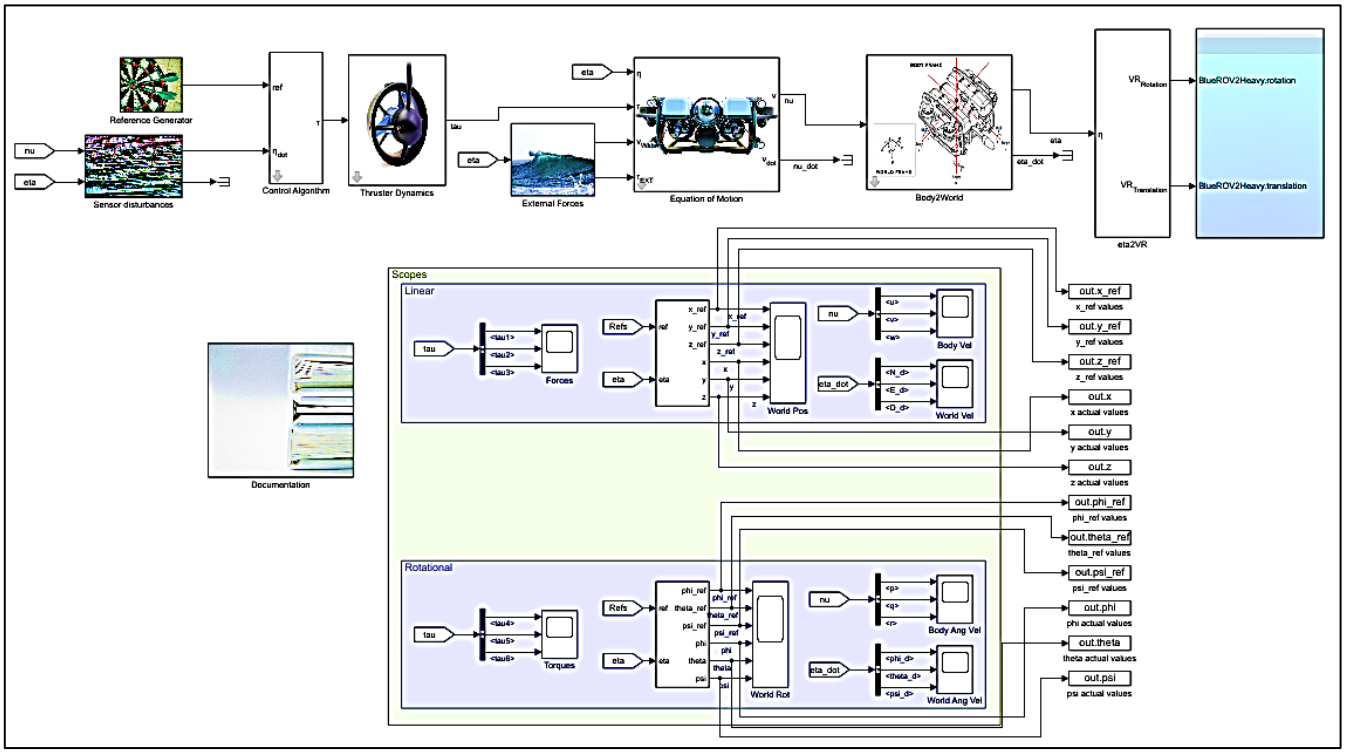

Fig. 8. Simulink diagram of the BlueROV2 open-source platform by [52]

TABLE III. THRUSTER CONFIGURATIONS OF THE BLUEROV2

Movement	τ_x	τ_y	τ_z	τ_ϕ	τ_θ	τ_ψ
Surge	0.7071	0.7071	-0.7071	-0.7071	0	0
Sway	-0.7071	0.7071	-0.7071	0.7071	0	0
Heave	0	0	0	0	-1	1
Roll	0	0	0	0	0	0
Pitch	0	0	0	0	0	0
Yaw	-0.1888	0.1888	0.1888	-0.1888	0	0

TABLE IV. CONTROL ALGORITHM PARAMETERS

PID Controller		
Movement	**Parameters**	**Values**
u	$K_P; K_I; K_D$	-10; 0.01; 0.1
v	$K_P; K_I; K_D$	-20; 0.05; 0.1
w	$K_P; K_I; K_D$	0.5; 0.01; 0.1
r	$K_P; K_I; K_D$	-2;0.01;0.1
SMC Controller		
Movement	**Parameters**	**Values**
u	K_1	1
v	K_2	1
w	K_3	1
r	K_4	1

VII. RESULTS

After implementing the parameters from TABLES I-IV, the next step is to conduct simulations under various conditions. These conditions included running the PID control algorithm without disturbances and with disturbances from ISW at intensities of 25%, 50%, 75%, and 100%. The same series of simulations is performed using the SMC control algorithm. All simulations were conducted over a 30-second duration. The results of these simulations for both the PID and SMC control algorithms are shown in Fig. 9 to Fig. 12.

A. PID Controller Results (in the Absence and the Presence of ISW Disturbances)

Fig. 9(a) shows a three-dimensional plot of the AUV's dynamic movement, with each axis representing the X, Y, and Z positions. Meanwhile, Fig. 9(b) to Fig. 9(e) display two-dimensional plots of the AUV's dynamic movement, where the X-axis represents time and the Y-axis represents position for each respective axis.

Fig. 9(a) shows the BlueROV2 tracking the reference trajectory (blue) using PID control without ISW disturbances. The actual path (red dashed) closely follows the reference, indicating accurate tracking. Fig. 9(b) through Fig. 9(e) offer a closer look at the BlueROV2's performance along the individual axes—x, y, z, and yaw (ψ)—providing a more detailed analysis. These figures reveal that the BlueROV2 consistently tracks its reference paths in the x, y, and z axes with precision. However, a minor oscillation is detected in the yaw (ψ) axis, as seen in Fig. 9(e). This oscillation occurs because the tuning values for each PID gain constant have not yet reached their best values. This highlights one of the key limitations of the PID control algorithm: there is no definitive formula for tuning the PID gain constants. The best values are usually determined through trial and error [75]. The lack of a systematic method for achieving ideal tuning often leads to suboptimal performance, where oscillations or delays in response may occur. Consequently, operators must experiment with different values to find the most effective settings, which can be time-consuming and may not always yield the desired precision [76][77]. This slight oscillation indicates a potential area where the yaw control could be further optimized to ensure smoother trajectory-tracking missions.

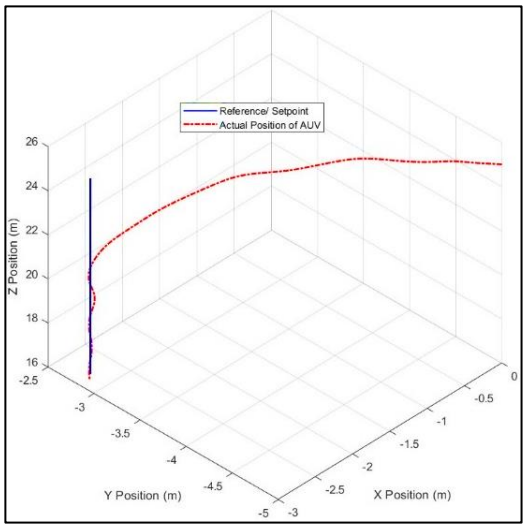

(a) The Three-Dimension (3D) Plot of the BlueROV2 Movement

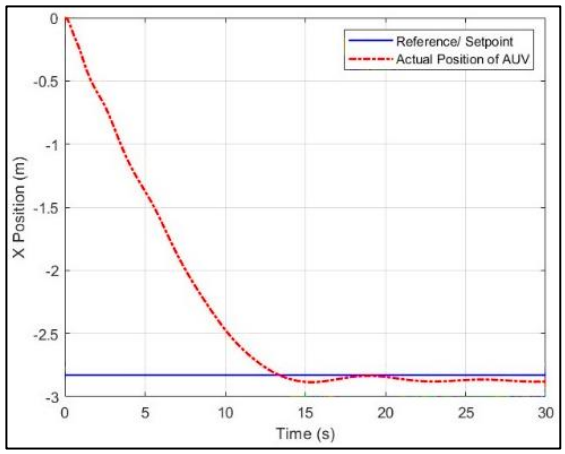

(b) The Two-Dimension Plot of BlueROV2 in Surge (x) Direction

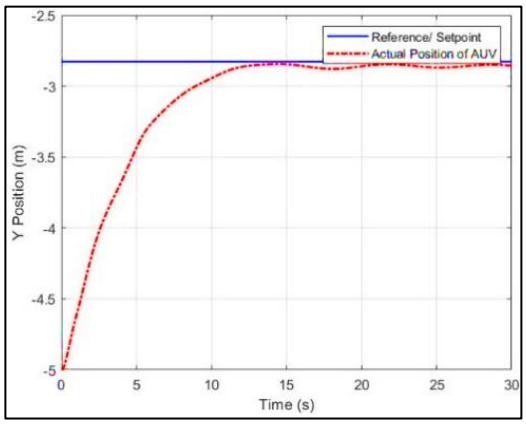

(c) The Two-Dimension Plot of BlueROV2 in Sway (y) Direction

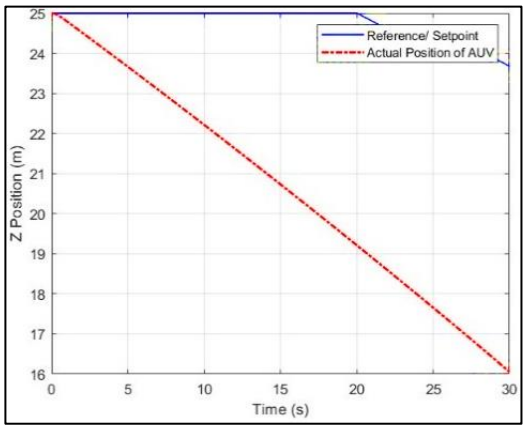

(d) The Two-Dimension Plot of BlueROV2 in Heave (z) Direction

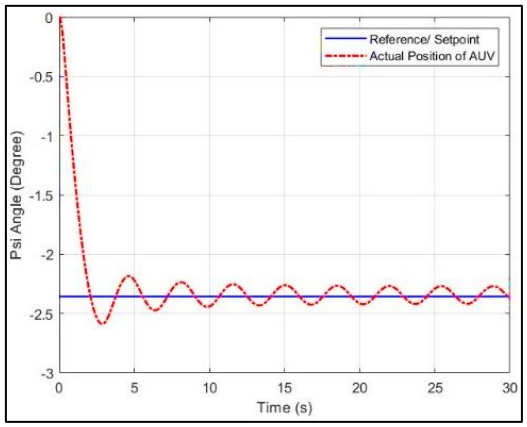

(e) The Two-Dimension Plot of BlueROV2 in Yaw (ψ) Direction

Fig. 9. Simulation results of BlueROV2 with PID control algorithm without ISW disturbances

The authors then introduced ISW disturbances into the simulation. A key objective of this paper is to assess the impact of ISW disturbances on the control performance of the BlueROV2. The results are shown in Fig. 10. Similar to the previous simulations, Fig. 10(a) displays a three-dimensional view of BlueROV2's performance using the PID control algorithm, but now with an ISW disturbance set at 25% of its maximum value (0.6725 m/s). Even with just 25% of the disturbance applied, the actual position of the BlueROV2 deviates significantly from the reference trajectory. This is consistent with the deviations seen along the individual axes, as shown in Fig. 10(b) through Fig. 10(e). These results show that the PID control algorithm cannot effectively counteract ISW disturbances, leading to inaccurate trajectory tracking. This highlights the need for more advanced control strategies to handle ISW disturbances and ensure precise trajectory-tracking missions.

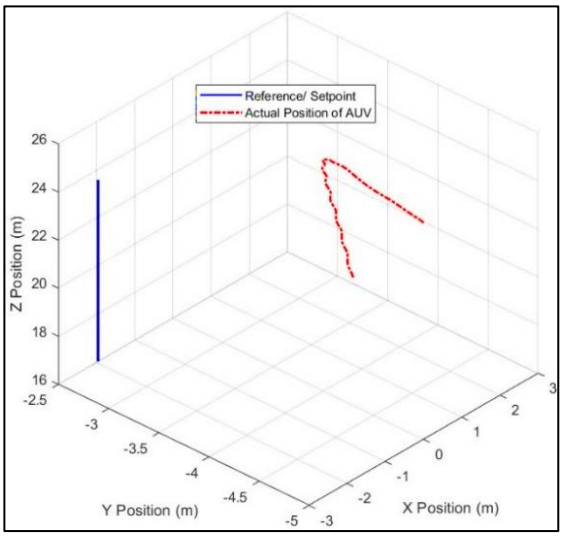

(a) The Three-Dimension (3D) Plot of the BlueROV2 Movement

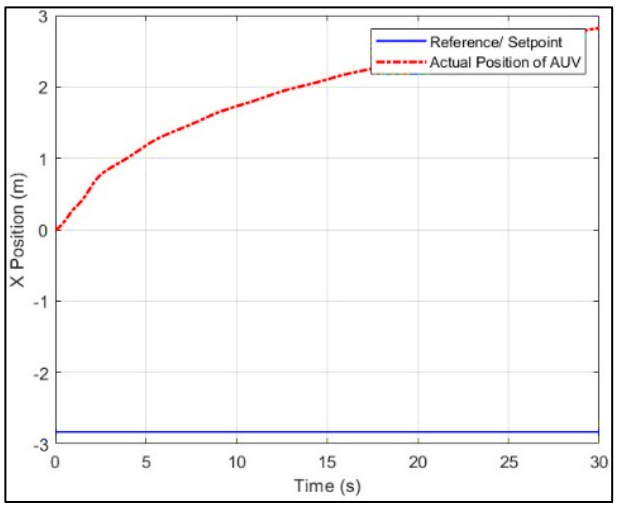

(b) The Two-Dimension Plot of BlueROV2 in Surge (x) Direction

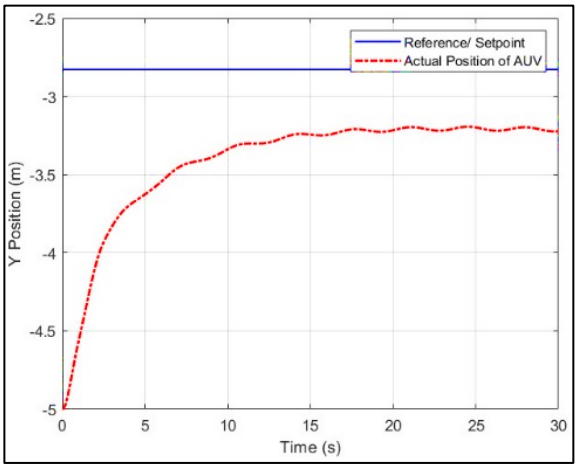

(c) The Two-Dimension Plot of BlueROV2 in Sway (y) Direction

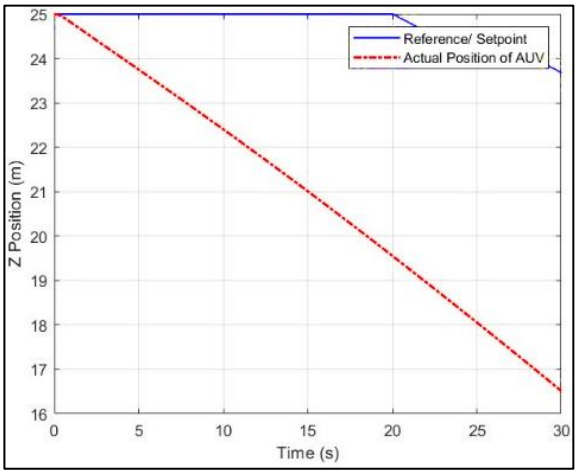

(d) The Two-Dimension Plot of BlueROV2 in Heave (z) Direction

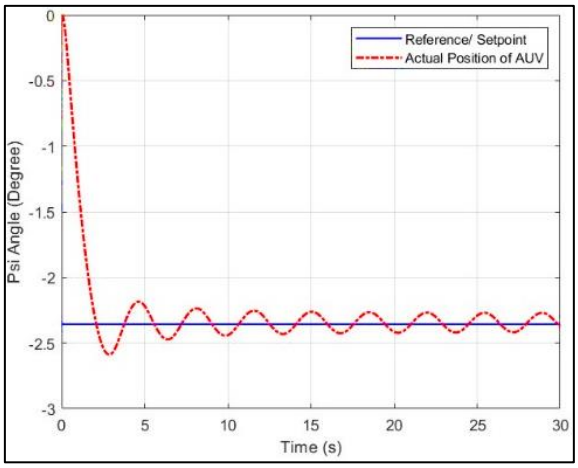

(e) The Two-Dimension Plot of BlueROV2 in Yaw (ψ) Direction

Fig. 10. Simulation results of BlueROV2 with PID control algorithm with 25% of ISW disturbances

B. SMC Controller Results (in the Absence and the Presence of ISW Disturbances)

Beyond the PID control algorithm, the authors also examined the effects of ISW disturbances using a different control strategy: SMC. SMC is recognized as a robust control method, frequently applied in both industrial settings and robotics, particularly for systems with nonlinear dynamics. This study tested the SMC algorithm's effectiveness in tracking trajectory when ISW disturbances were introduced. The simulation results using the SMC control algorithm without ISW disturbances are shown in Fig. 11.

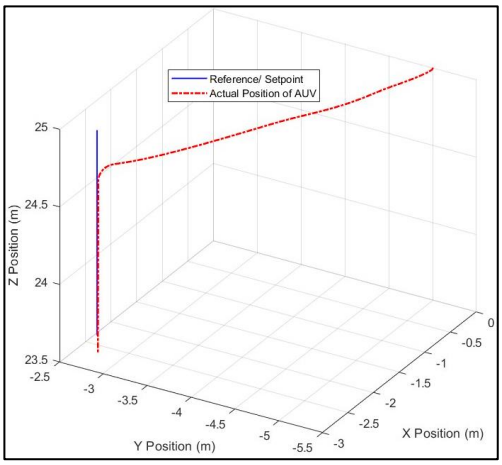

(a) The Three-Dimension (3D) Plot of the BlueROV2 Movement

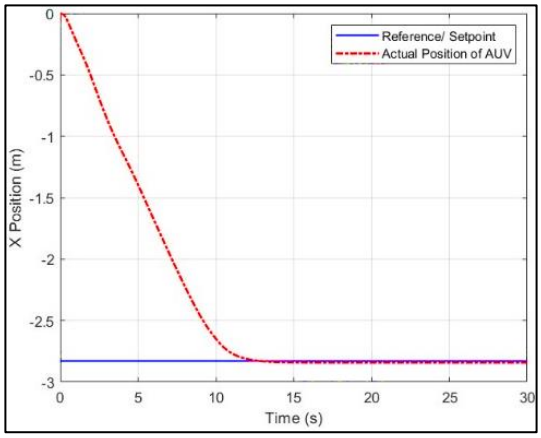

(b) The Two-Dimension Plot of BlueROV2 in Surge (x) Direction

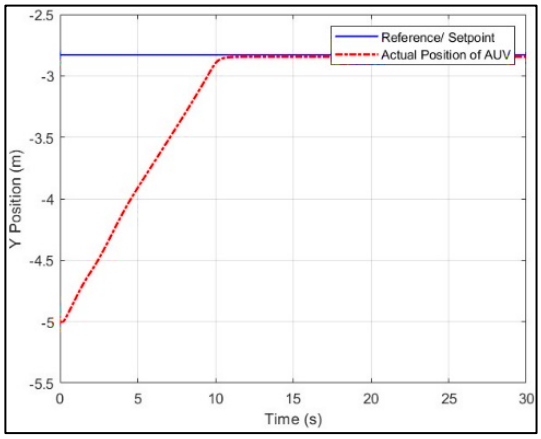

(c) The Two-Dimension Plot of BlueROV2 in Sway (y) Direction

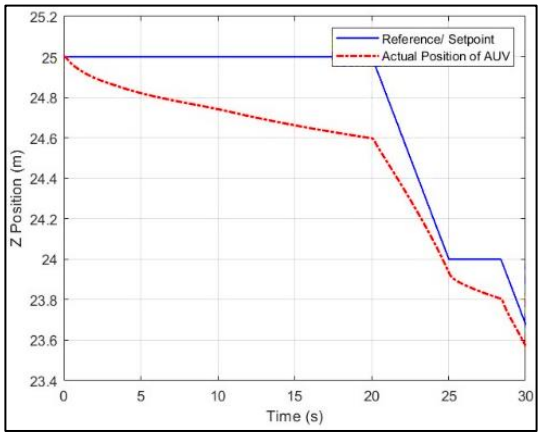

(d) The Two-Dimension Plot of BlueROV2 in Heave (z) Direction

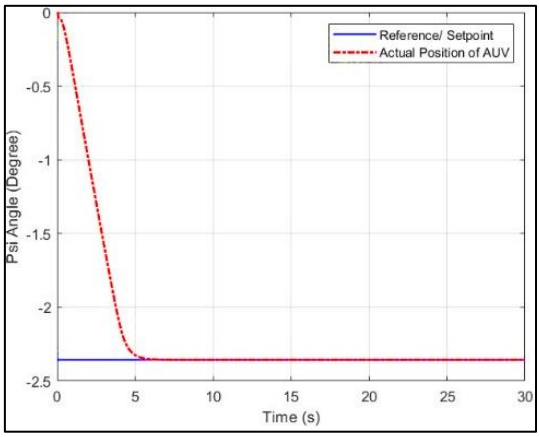

(e) The Two-Dimension Plot of BlueROV2 in Yaw (ψ) Direction

Fig. 11. Simulation results of BlueROV2 with SMC control algorithm without ISW disturbances

Fig. 11 demonstrates that the SMC algorithm delivers overall solid performance in trajectory tracking. Notably, the oscillations in the yaw (ψ) The movement observed in Fig. 9(e) and Fig. 10(e) do not appear in Fig. 11(e). This advantage arises because the SMC control algorithm directly incorporates the mathematical model of the AUV's dynamic system into its control strategy. Unlike PID, where tuning the gain constants often involves a trial-and-error process, the tuning in SMC can be formulated more precisely. Additionally, as the gain constants in SMC increase, the dynamic system becomes more robust [73][78][79], allowing the AUV to handle disturbances better and maintain stability even in challenging conditions. This level of robustness is what makes SMC superior in managing complex dynamic systems like AUVs. This improvement can be attributed to SMC's design, which is well-suited for managing the BlueROV2's nonlinear characteristics. These findings suggest that SMC provides a more reliable control solution, offering better stability and accuracy in trajectory tracking than the PID algorithm.

The 25% ISW disturbance factor was then applied to the SMC control algorithm, with the results shown in Fig 12. Fig. 12(a) reveals that the BlueROV2, under SMC control, also struggled with trajectory tracking when faced with ISW disturbances, much like the earlier results with the PID algorithm in Fig. 10(a). This is further confirmed by the performance analysis across the individual axes, presented in Fig. 12(b) through Fig. 12(e). These findings suggest that even the robust SMC algorithm cannot effectively manage the ISW disturbances in the BlueROV2 system.

C. Comparative Analysis

The authors also conducted a quantitative analysis based on Fig. 9 through Fig. 12. This analysis involved calculating the RMSE for each axis—x, y, z, and ψ. The RMSE values measure the error or deviation, with higher RMSE values indicating a more significant error. The RMSE values for each axis, corresponding to both control algorithms—PID and SMC—are presented in Table V and Table VI, respectively.

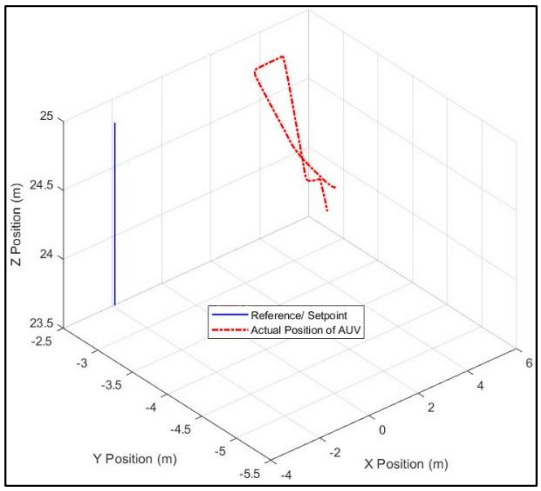

(a) The Three-Dimension (3D) Plot of the BlueROV2 Movement

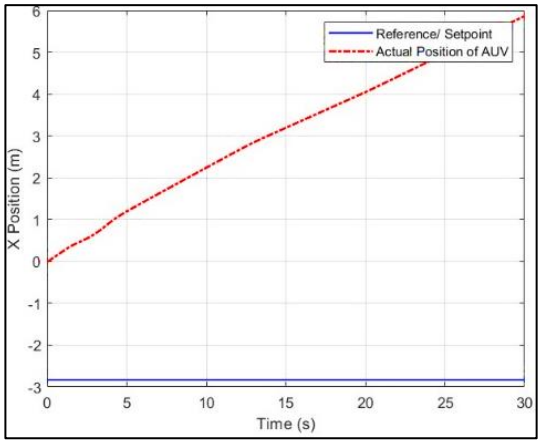

(b) The Two-Dimension Plot of BlueROV2 in Surge (x) Direction

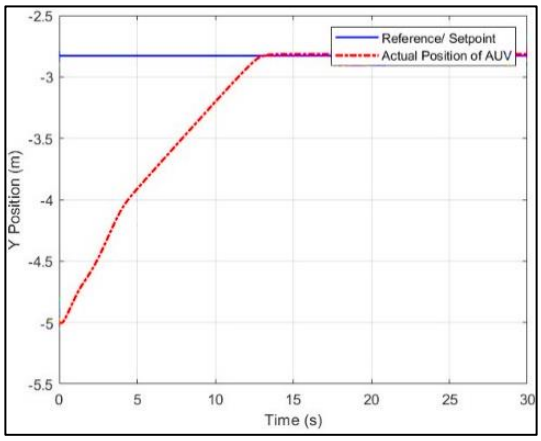

(c) The Two-Dimension Plot of BlueROV2 in Sway (y) Direction

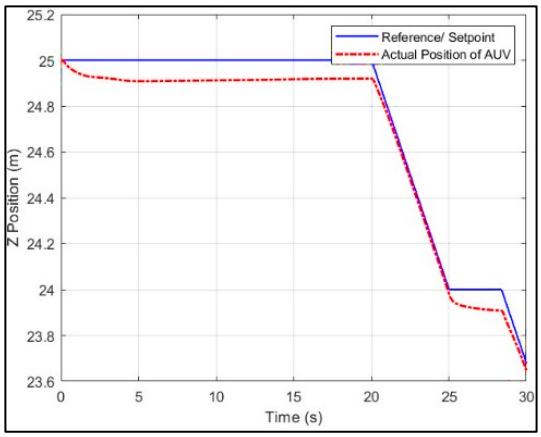

(d) The Two-Dimension Plot of BlueROV2 in Heave (z) Direction

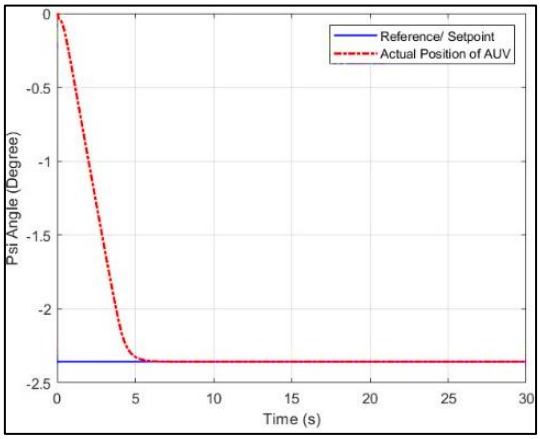

(e) The Two-Dimension Plot of BlueROV2 in Yaw (ψ) Direction

Fig. 12. Simulation results of BlueROV2 with SMC control algorithm with 25% of ISW disturbances

TABLE V. PID CONTROLLER RMSE VALUES

Direction	RMSE Values				
	0% ISW	25% ISW	50% ISW	75% ISW	100% ISW
x	0.9612	4.8086	13.9832	70.1093	87.3401
y	0.5782	0.6900	0.7305	15.8533	11.8225
z	4.6581	4.3709	3.5642	49.8421	63.2708
ψ	0.3576	0.3577	0.3611	0.5043	0.6324

TABLE VI. SMC CONTROLLER RMSE VALUES

Direction	RMSE Values				
	0% ISW	25% ISW	50% ISW	75% ISW	100% ISW
x	0.9590	6.1519	15.4339	68.4595	81.0705
y	0.7352	0.7487	0.7662	11.1607	12.9284
z	0.2490	0.0747	0.0134	45.0996	55.0180
ψ	0.5491	0.5492	0.5491	0.7033	0.8728

Table V and Table VI present the RMSE values for each axis under the PID and SMC control algorithms. As shown in these tables, the authors did not limit the analysis to a 25% ISW disturbance factor; instead, they progressively increased the ISW intensity to 100% in increments of 25%. This approach was taken to investigate further the impact of increasing ISW levels on the RMSE values for each control algorithm, providing insights that could inform future control algorithm development. The tables reveal a clear trend: as the ISW intensity increases, the RMSE values for both control algorithms also rise. To visualize this trend, the RMSE values from Table V and Table VI are plotted in Fig. 12.

Fig. 13 shows that the RMSE increase is not linear; it is nearly exponential, particularly along the X-axis for both control algorithms, despite the linear increase in ISW disturbance (consistent 25% increments). A striking example of this can be seen when the ISW intensity is raised from 50% to 75%. Initially, at 50% ISW, the RMSE values are 18.9832 for the PID algorithm and 15.4339 for the SMC algorithm. However, when the ISW intensity reaches 75%, the RMSE values surge dramatically to 70.1093 for PID and 68.4595 for SMC, as shown in Table V and Table VI and illustrated in Fig. 13. This analysis underscores the significant impact of ISW disturbances on the trajectory-tracking performance of both the PID and SMC control algorithms. The exponential increase in RMSE, particularly with higher ISW intensities, highlights the limitations of these control strategies in effectively managing such disturbances. These findings suggest a critical need for developing more advanced or adaptive control algorithms that can better handle the nonlinear effects introduced by ISW, ensuring more reliable and accurate performance of underwater vehicles like the BlueROV2 in challenging environments.

The exponential increase in RMSE under higher ISW intensity is due to the nonlinear nature of ISW disturbances and the limitations of conventional control algorithms like PID and SMC in handling such nonlinearities. As ISW intensity rises, the forces acting on the AUV become more complex and unpredictable, causing small errors to compound rapidly [80][81]. This results in greater trajectory deviations that grow exponentially, especially at higher disturbance levels. The control algorithms struggle to manage the increasingly chaotic dynamics, highlighting the need for more advanced or adaptive control methods to handle the nonlinear effects of ISW better and ensure accurate performance in challenging underwater environments.

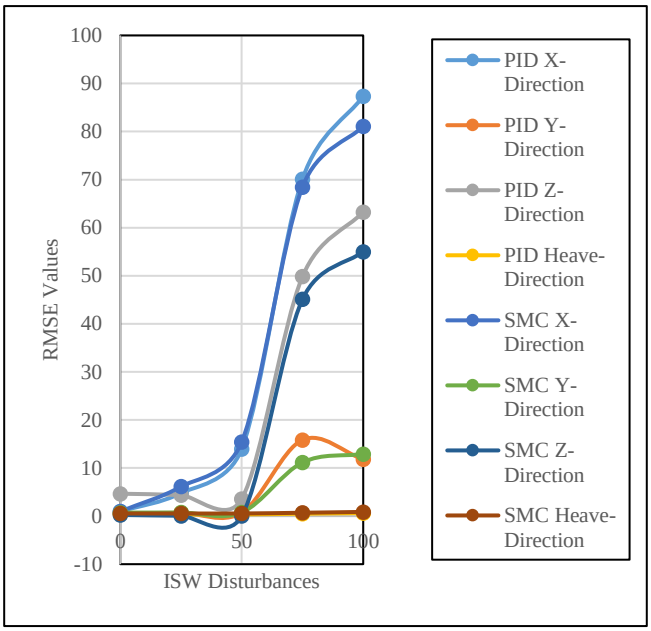

Fig. 13. A Visual representation of the RMSE values increases with the rising ISW intensity derived from Table V and Table VI

VIII. CONCLUSIONS

This study assessed the performance of PID and SMC control algorithms for an AUV under Internal Solitary Wave (ISW) disturbances using real-world data from the Bali Deep Sea. Simulations demonstrated that both algorithms struggled to maintain accurate trajectory tracking, with Root Mean Square Error (RMSE) values increasing exponentially as ISW intensity rose. Notably, neither PID nor SMC algorithms fully compensated for nonlinear disturbances at higher ISW intensities, revealing critical limitations in conventional control approaches.

A key contribution of this research is the identification of ISWs as significant destabilizing factors for AUV control in deep-sea environments. By quantifying the exponential rise in RMSE under increasing ISW intensities, this study advances the theoretical understanding of how ISWs interact with control systems. The research highlights the inadequacy of current linear and sliding mode control methods in managing these complex nonlinear disturbances.

These findings underscore the necessity for more advanced control algorithms, particularly Nonlinear Model Predictive Control (NMPC), which can handle the dynamic, nonlinear characteristics of ISWs. NMPC's ability to adapt to real-time environmental changes and optimize control inputs in the presence of multiple constraints positions it as a promising solution for future AUV operations in challenging underwater conditions.

Future work will focus on implementing and testing NMPC in real-world scenarios to further validate these findings and address the limitations of existing algorithms in deep-sea exploration.

ACKNOWLEDGMENT

The authors express gratitude to the Ministry of Education, Culture, Research, and Technology of the Republic of Indonesia, in collaboration with Institut Teknologi Sepuluh Nopember, for the State University Operational Assistance Program for Doctoral Dissertation Research, under Number: 027/E5/PG.02.00.PL/2024, which provided material support throughout the research process. Additionally, the author thanks all team members, specifically the Beehive Intelligent Robotics Laboratory (BIRL) and Beehive Drones, for their funding and significant technical assistance in this study.

NOMENCLATURE

Symbols	Description
M_{RB}	The force and moment due to the acceleration of ROV rigid body mass
M_A	The water added mass around the ROV body
m	The total mass of ROV
x_G, y_G, z_G	The position of the center of gravity of the ROV
I_x, I_y, I_z	The moment of inertia of each axis
I_{ij}	The product for i, j plane that measures the imbalance of mass distribution.
$X_{\dot{u}}, Y_{\dot{v}}, Z_{\dot{w}}$	The added mass in *x*, *y*, *z* direction due to translation in water
$K_{\dot{p}}, M_{\dot{q}}, N_{\dot{r}}$	The increased inertia about x, y, z direction due to rotation in water
C_{RB}	The Coriolis force matrix of the rigid body
C_A	The Coriolis added mass
D	The hydrodynamic damping
$g(\eta)$	The hydrostatic restoring forces vector
τ	The propulsion forces vector
τ_{ext}	The external disturbances
$X_{u\|u}, Y_{v\|v}, Z_{w\|w}$	The quadratic damping of each axis in linear direction (x, y, z)
$K_{p\|p}, M_{q\|q}, N_{r\|r}$	The quadratic damping of each axis in angular direction (ϕ, θ, ψ)
X_u, Y_v, Z_w	The linear damping of each axis in linear direction (x, y, z)
K_p, M_q, N_r	The linear damping of each axis in angular direction (ϕ, θ, ψ)
W	The weight forces of ROV
B	The buoyancy forces of ROV
$\vec{R}$	The transformation matrix of the linear velocity (u, v, w)
$\vec{T}$	The transformation matrix of the angular velocity (p, q, r)
v_{ISW}	The ISW velocity
g	Gravity constants
h_1, h_2	The thickness of the upper and lower water density
ρ_1, ρ_2	The relative layer density of the upper and lower water
e_x, e_y, e_z	The error position for PID and SMC controller
K_P, K_I, K_D	The gain constants for PID controller
K_1, K_2, K_3, K_4	The gain constants for SMC controller

REFERENCES

[1] K. L. C. Bell *et al.*, "Exposing inequities in deep-sea exploration and research: results of the 2022 Global Deep-Sea Capacity Assessment," *Front. Mar. Sci.*, vol. 10, Aug. 2023, doi: 10.3389/fmars.2023.1217227.

[2] D. L. McLean *et al.*, "Enhancing the Scientific Value of Industry Remotely Operated Vehicles (ROVs) in Our Oceans," *Front. Mar. Sci.*, vol. 7, Apr. 2020, doi: 10.3389/fmars.2020.00220.

[3] D. J. Amon *et al.*, "My Deep Sea, My Backyard: a pilot study to build capacity for global deep-ocean exploration and research," *Philos. Trans. R. Soc. B Biol. Sci.*, vol. 377, no. 1854, Jul. 2022, doi: 10.1098/rstb.2021.0121.

[4] O. A. Aguirre-Castro *et al.*, "Design and Construction of an ROV for Underwater Exploration," *Sensors*, vol. 19, no. 24, p. 5387, Dec. 2019, doi: 10.3390/s19245387.

[5] E. I. van Putten *et al.*, "History matters: societal acceptance of deep-sea mining and incipient conflicts in Papua New Guinea," *Marit. Stud.*, vol. 22, no. 3, p. 32, Sep. 2023, doi: 10.1007/s40152-023-00318-0.

[6] M. Vigo *et al.*, "ROV-based monitoring of passive ecological recovery in a deep-sea no-take fishery reserve," *Sci. Total Environ.*, vol. 883, p. 163339, Jul. 2023, doi: 10.1016/j.scitotenv.2023.163339.

[7] Y. Zhang *et al.*, "Characteristics of Internal Solitary Waves in the Timor Sea Observed by SAR Satellite," *Remote Sens.*, vol. 15, no. 11, p. 2878, Jun. 2023, doi: 10.3390/rs15112878.

[8] X. Huang *et al.*, "An extreme internal solitary wave event observed in the northern South China Sea," *Sci. Rep.*, vol. 6, no. 1, p. 30041, Jul. 2016, doi: 10.1038/srep30041.

[9] I. W. G. A. Karang, Chonnaniyah, and T. Osawa, "Internal solitary wave observations in the Flores Sea using the Himawari-8 geostationary satellite," *Int. J. Remote Sens.*, vol. 41, no. 15, pp. 5726–5742, Aug. 2020, doi: 10.1080/01431161.2019.1693079.

[10] F. Syamsudin *et al.*, "Observing Internal Solitary Waves in the Lombok Strait by Coastal Acoustic Tomography," *Geophys. Res. Lett.*, vol. 46, no. 17–18, pp. 10475–10483, Sep. 2019, doi: 10.1029/2019GL084595.

[11] B. Zhao *et al.*, "Internal solitary waves generated by a moving bottom disturbance," *J. Fluid Mech.*, vol. 963, p. A32, May 2023, doi: 10.1017/jfm.2023.355.

[12] L. Sun *et al.*, "Internal solitary waves in the central Andaman sea observed by combining mooring data and satellite remote sensing," *Cont. Shelf Res.*, vol. 277, p. 105249, Jun. 2024, doi: 10.1016/j.csr.2024.105249.

[13] S. Liu *et al.*, "Multi-Parameter Influence Analysis of Interaction Between Internal Solitary Wave and Fixed Submerged Body," *China Ocean Eng.*, vol. 37, no. 6, pp. 934–947, Dec. 2023, doi: 10.1007/s13344-023-0078-3.

[14] Z. Bingul and K. Gul, "Intelligent-PID with PD Feedforward Trajectory Tracking Control of an Autonomous Underwater Vehicle," *Machines*, vol. 11, no. 2, p. 300, Feb. 2023, doi: 10.3390/machines11020300.

[15] Y. Wang, Y. Hou, Z. Lai, L. Cao, W. Hong, and D. Wu, "An adaptive PID controller for path following of autonomous underwater vehicle based on Soft Actor–Critic," *Ocean Eng.*, vol. 307, p. 118171, Sep. 2024, doi: 10.1016/j.oceaneng.2024.118171.

[16] J. Guerrero, J. Torres, V. Creuze, A. Chemori, and E. Campos, "Saturation based nonlinear PID control for underwater vehicles: Design, stability analysis and experiments," *Mechatronics*, vol. 61, pp. 96–105, 2019, doi: 10.1016/j.mechatronics.2019.06.006.

[17] P. V. Patil, M. K. Khan, M. Korulla, V. Nagarajan, and O. P. Sha, "Design optimization of an AUV for performing depth control maneuver," *Ocean Eng.*, vol. 266, no. 5, 2022, doi: 10.1016/j.oceaneng.2022.112929.

[18] M. T. Muhssin, M. N. Ajaweed, and S. K. Khalaf, "Optimal control of underwater vehicle using LQR controller driven by new matrix decision control algorithm," *Int. J. Dyn. Control*, vol. 11, no. 6, pp. 2911–2923, Dec. 2023, doi: 10.1007/s40435-023-01186-6.

[19] A. Sir Elkhatem and S. Naci Engin, "Robust LQR and LQR-PI control strategies based on adaptive weighting matrix selection for a UAV position and attitude tracking control," *Alexandria Eng. J.*, vol. 61, no. 8, pp. 6275–6292, Aug. 2022, doi: 10.1016/j.aej.2021.11.057.

[20] Y. Duan, X. Xiang, C. Liu, and L. Yang, "Double-loop LQR depth tracking control of underactuated AUV: Methodology and comparative

experiments," *Ocean Eng.*, vol. 300, p. 117410, May 2024, doi: 10.1016/j.oceaneng.2024.117410.

[21] Q. Zhu, H. Shang, X. Lu, and Y. Chen, "Adaptive sliding mode tracking control of underwater vehicle-manipulator systems considering dynamic disturbance," *Ocean Eng.*, vol. 291, p. 116300, Jan. 2024, doi: 10.1016/j.oceaneng.2023.116300.

[22] Y. Sun, P. Chai, G. Zhang, T. Zhou, and H. Zheng, "Sliding Mode Motion Control for AUV with Dual-Observer Considering Thruster Uncertainty," *J. Mar. Sci. Eng.*, vol. 10, no. 3, p. 349, Mar. 2022, doi: 10.3390/jmse10030349.

[23] D. Wang *et al.*, "Sliding mode heading control for AUV based on continuous hybrid model-free and model-based reinforcement learning," *Appl. Ocean Res.*, vol. 118, p. 102960, Jan. 2022, doi: 10.1016/j.apor.2021.102960.

[24] H.-H. Kim, M. C. Lee, H.-J. Cho, J.-H. Hwang, and J.-S. Won, "SMCSPO-Based Robust Control of AUV in Underwater Environments including Disturbances," *Appl. Sci.*, vol. 11, no. 22, p. 10978, Nov. 2021, doi: 10.3390/app112210978.

[25] A. Sahoo, S. K. Dwivedy, and P. S. Robi, "Adaptive Fuzzy PID Controller for A Compact Autonomous Underwater Vehicle," in *Global Oceans 2020: Singapore – U.S. Gulf Coast*, pp. 1–6, 2020, doi: 10.1109/IEEECONF38699.2020.9389483.

[26] T. Liu, J. Zhao, J. Huang, Z. Li, L. Xu, and B. Zhao, "Research on model predictive control of autonomous underwater vehicle based on physics informed neural network modeling," *Ocean Eng.*, vol. 304, p. 117844, Jul. 2024, doi: 10.1016/j.oceaneng.2024.117844.

[27] J. Yao, J. Yang, C. Zhang, J. Zhang, and T. Zhang, "Autonomous Underwater Vehicle Trajectory Prediction with the Nonlinear Kepler Optimization Algorithm–Bidirectional Long Short-Term Memory–Time-Variable Attention Model," *J. Mar. Sci. Eng.*, vol. 12, no. 7, p. 1115, Jul. 2024, doi: 10.3390/jmse12071115.

[28] J. Zheng, L. Song, L. Liu, W. Yu, Y. Wang, and C. Chen, "Fixed-time sliding mode tracking control for autonomous underwater vehicles," *Appl. Ocean Res.*, vol. 117, p. 102928, Dec. 2021, doi: 10.1016/j.apor.2021.102928.

[29] B. Li, X. Gao, H. Huang, and H. Yang, "Improved adaptive twisting sliding mode control for trajectory tracking of an AUV subject to uncertainties," *Ocean Eng.*, vol. 297, p. 116204, Apr. 2024, doi: 10.1016/j.oceaneng.2023.116204.

[30] L. Ibarra, A. Rosales, P. Ponce, and A. Molina, "Adaptive SMC based on the dynamic containment of the sliding variable," *J. Franklin Inst.*, vol. 358, no. 2, pp. 1422–1447, Jan. 2021, doi: 10.1016/j.jfranklin.2020.12.005.

[31] H. Chen, G. Tang, S. Wang, W. Guo, and H. Huang, "Adaptive fixed-time backstepping control for three-dimensional trajectory tracking of underactuated autonomous underwater vehicles," *Ocean Eng.*, vol. 275, p. 114109, May 2023, doi: 10.1016/j.oceaneng.2023.114109.

[32] Y. Peng, L. Guo, and Q. Meng, "Backstepping Control Strategy of an Autonomous Underwater Vehicle Based on Probability Gain," *Mathematics*, vol. 10, no. 21, p. 3958, Oct. 2022, doi: 10.3390/math10213958.

[33] S. An, L. Wang, and Y. He, "Robust fixed-time tracking control for underactuated AUVs based on fixed-time disturbance observer," *Ocean Eng.*, vol. 266, p. 112567, Dec. 2022, doi: 10.1016/j.oceaneng.2022.112567.

[34] M. Bjaoui, B. Khiari, R. Benadli, M. Memni, and A. Sellami, "Practical Implementation of the Backstepping Sliding Mode Controller MPPT for a PV-Storage Application," *Energies*, vol. 12, no. 18, p. 3539, Sep. 2019, doi: 10.3390/en12183539.

[35] Y. Liu, F. Li, and B. Sun, "Self-Tuning Backstepping Control with Kalman-like Filter for High-Precision Control of Automotive Electronic Throttle," *Electronics*, vol. 12, no. 13, p. 2938, Jul. 2023, doi: 10.3390/electronics12132938.

[36] J. Na, Y. Li, Y. Huang, G. Gao, and Q. Chen, "Output Feedback Control of Uncertain Hydraulic Servo Systems," *IEEE Trans. Ind. Electron.*, vol. 67, no. 1, pp. 490–500, Jan. 2020, doi: 10.1109/TIE.2019.2897545.

[37] T. Wang, X. Huang, W. Zhao, S. Zheng, Y. Yang, and J. Tian, "Internal Solitary Wave Activities near the Indonesian Submarine Wreck Site Inferred from Satellite Images," *J. Mar. Sci. Eng.*, vol. 10, no. 2, p. 197, Feb. 2022, doi: 10.3390/jmse10020197.

[38] Y. Stepanyants, "How internal waves could lead to wreck American and Indonesian submarines?," *arXiv preprint arXiv:2107.00828*, 2021.

[39] Y.-Y. Chen, C.-Y. Lee, Y.-X. Huang, and T.-T. Yu, "Control Allocation Design for Torpedo-Like Underwater Vehicles with Multiple Actuators," *Actuators*, vol. 11, no. 4, p. 104, Mar. 2022, doi: 10.3390/act11040104.

[40] R. Gabl *et al.*, "Hydrodynamic loads on a restrained ROV under waves and current," *Ocean Eng.*, vol. 234, p. 109279, Aug. 2021, doi: 10.1016/j.oceaneng.2021.109279.

[41] S. Heshmati-Alamdari, C. P. Bechlioulis, G. C. Karras, and K. J. Kyriakopoulos, "Cooperative Impedance Control for Multiple Underwater Vehicle Manipulator Systems Under Lean Communication," *IEEE J. Ocean. Eng.*, vol. 46, no. 2, pp. 447–465, Apr. 2021, doi: 10.1109/JOE.2020.2989603.

[42] Z. Zhang, Q. Wang, and S. Zhang, "Review of Computational Fluid Dynamics Analysis in Biomimetic Applications for Underwater Vehicles," *Biomimetics*, vol. 9, no. 2, p. 79, Jan. 2024, doi: 10.3390/biomimetics9020079.

[43] S. Song, J. Kim, T. Kim, Y. Song, and S.-C. Yu, "Development of a Biomimetic Underwater Robot for Bottom Inspection of Marine Structures," *Int. J. Control. Autom. Syst.*, vol. 21, no. 12, pp. 4041–4056, Dec. 2023, doi: 10.1007/s12555-023-0250-9.

[44] K. D. Wahyuadnyana, K. Indriawati, P. A. Darwito, A. N. Aufa, and H. Tnunay, "Comparative Numerical Analysis of Torpedo-Shaped and Cubic Symmetrical Autonomous Underwater Vehicles in the Context of Indonesian Marine Environments," *Math. Model. Eng. Probl.*, vol. 10, no. 6, Dec. 2023, doi: 10.18280/mmep.100601.

[45] Blue Robotics, "Enabling Ocean Exploration." *Blue Robotics*, [Online]. Available: https://bluerobotics.com/

[46] E. G. Garrison *et al.*, "'Scouring for Prehistory'—An Opportunistic Methodology for Sea Floor Archaeology," *Heritage*, vol. 7, no. 7, pp. 3417–3428, Jun. 2024, doi: 10.3390/heritage7070161.

[47] Y. Cao, B. Li, Q. Li, A. A. Stokes, D. M. Ingram, and A. Kiprakis, "A Nonlinear Model Predictive Controller for Remotely Operated Underwater Vehicles With Disturbance Rejection," *IEEE Access*, vol. 8, pp. 158622–158634, 2020, doi: 10.1109/ACCESS.2020.3020530.

[48] Q. Li, Y. Cao, B. Li, D. M. Ingram, and A. Kiprakis, "Numerical Modelling and Experimental Testing of the Hydrodynamic Characteristics for an Open-Frame Remotely Operated Vehicle," *J. Mar. Sci. Eng.*, vol. 8, no. 9, p. 688, Sep. 2020, doi: 10.3390/jmse8090688.

[49] T. I. Fossen, *Marine control systems: guidance, navigation and control of ships, rigs and underwater vehicles*. Norway: Marine Cybernetics, 2002.

[50] T. I. Fossen, *Handbook of marine craft hydrodynamics and motion control*. Wiley, 2011.

[51] J. Du, D. Zhou, and S. Arai, "Hybrid Layer of Improved Interfered Fluid Dynamic System and Nonlinear Model Predictive Control for Navigation and Control of Autonomous Underwater Vehicles," *J. Mar. Sci. Eng.*, vol. 11, no. 10, p. 2014, Oct. 2023, doi: 10.3390/jmse11102014.

[52] M. von Benzon, F. F. Sørensen, E. Uth, J. Jouffroy, J. Liniger, and S. Pedersen, "An Open-Source Benchmark Simulator: Control of a BlueROV2 Underwater Robot," *J. Mar. Sci. Eng.*, vol. 10, no. 12, p. 1898, Dec. 2022, doi: 10.3390/jmse10121898.

[53] M. Folley, "The Wave Energy Resource," in *Handbook of Ocean Wave Energy, 7th ed., Ocean Engineering & Oceanograhy*, pp. 43–79, 2017, doi: 10.1007/978-3-319-39889-1_3.

[54] G. O. Abessolo *et al.*, "Wave influence on altimetry sea level at the coast," *Coast. Eng.*, vol. 180, p. 104275, Mar. 2023, doi: 10.1016/j.coastaleng.2022.104275.

[55] P. V Khalishah, Y. Naulita, and U. Hernawan, "Characteristics of North Pacific water masses in the Bali Sea," *IOP Conf. Ser. Earth Environ. Sci.*, vol. 1251, no. 1, p. 012039, Oct. 2023, doi: 10.1088/1755-1315/1251/1/012039.

[56] A. K. Mandal, M. Seemanth, and R. Ratheesh, "Characterization of internal solitary waves in the Andaman Sea and Arabian Sea using EOS-04 and sentinel observations," *Int. J. Remote Sens.*, vol. 45, no. 4, pp. 1201–1219, Feb. 2024, doi: 10.1080/01431161.2024.2307322.

[57] P. Peng *et al.*, "Analysis of the Differences in Internal Solitary Wave Characteristics Retrieved from Synthetic Aperture Radar Images under

Different Background Environments in the Northern South China Sea," *Remote Sens.*, vol. 15, no. 14, p. 3624, Jul. 2023, doi: 10.3390/rs15143624.

[58] Q. Gong, L. Chen, Y. Diao, X. Xiong, J. Sun, and X. Lv, "On the identification of internal solitary waves from moored observations in the northern South China Sea," *Sci. Rep.*, vol. 13, no. 1, p. 3133, Feb. 2023, doi: 10.1038/s41598-023-28565-5.

[59] N. W. Asmoro, W. S. Pranowo, Nurhidayat, J. Setiyadi, A. I. Santoso, and I. W. Sumardana E Putra, "Analysis of internal wave in the Buru Island coastal waters, Banda Sea, Indonesia," *Kuwait J. Sci.*, vol. 51, no. 3, p. 100238, Jul. 2024, doi: 10.1016/j.kjs.2024.100238.

[60] S. G. Hartharn-Evans, M. Stastna, and M. Carr, "Dense pulses formed from fissioning internal waves," *Environ. Fluid Mech.*, vol. 23, no. 2, pp. 389–405, Apr. 2023, doi: 10.1007/s10652-022-09894-x.

[61] S. G. Hartharn-Evans, M. Carr, and M. Stastna, "Interactions Between Internal Solitary Waves and Sea Ice," *J. Geophys. Res. Ocean.*, vol. 129, no. 1, Jan. 2024, doi: 10.1029/2023JC020175.

[62] A. Katavouta, J. A. Polton, J. D. Harle, and J. T. Holt, "Effect of Tides on the Indonesian Seas Circulation and Their Role on the Volume, Heat and Salt Transports of the Indonesian Throughflow," *J. Geophys. Res. Ocean.*, vol. 127, no. 8, pp. 1–29, Aug. 2022, doi: 10.1029/2022JC018524.

[63] M. R. Iskandar and T. Suga, "Change in Salinity of Indonesian Upper Water in the Southeastern Indian Ocean during Argo Period," *Heliyon*, vol. 8, no. 9, p. e10430, Sep. 2022.

[64] M. A. Wibowo *et al.*, "Understanding the Mechanism of Currents through the Malacca Strait Study Case 2020 – 2022 : Mean state, Seasonal and Monthly Variation," *IOP Conf. Ser. Earth Environ. Sci.*, vol. 1118, no. 1, p. 012069, Dec. 2022, doi: 10.1088/1755-1315/1118/1/012069.

[65] A. Latif, K. Shankar, and P. T. Nguyen, "Legged Fire Fighter Robot Movement Using PID," *J. Robot. Control*, vol. 1, no. 1, 2020, doi: 10.18196/jrc.1104.

[66] A. Latif, A. Z. Arfianto, H. A. Widodo, R. Rahim, and E. T.Helmy, "Motor DC PID System Regulator for Mini Conveyor Drive Based-on Matlab," *J. Robot. Control*, vol. 1, no. 6, 2020, doi: 10.18196/jrc.1636.

[67] M. Samuel, M. Mohamad, M. Hussein, and S. M. Saad, "Lane Keeping Maneuvers Using Proportional Integral Derivative (PID) and Model Predictive Control (MPC)," *J. Robot. Control*, vol. 2, no. 2, 2021, doi: 10.18196/jrc.2256.

[68] F. Santoso, M. A. Garratt, and S. G. Anavatti, "Hybrid PD-Fuzzy and PD Controllers for Trajectory Tracking of a Quadrotor Unmanned Aerial Vehicle: Autopilot Designs and Real-Time Flight Tests," *IEEE Trans. Syst. Man, Cybern. Syst.*, vol. 51, no. 3, pp. 1817–1829, 2021, doi: 10.1109/TSMC.2019.2906320.

[69] L. Bauersfeld, L. Spannagl, G. Ducard, and C. Onder, "MPC Flight Control for a Tilt-Rotor VTOL Aircraft," *IEEE Trans. Aerosp. Electron. Syst.*, vol. 57, no. 4, pp. 2395–2409, 2021, doi: 10.1109/TAES.2021.3061819.

[70] N. Xuan-Mung and S. K. Hong, "Improved altitude control algorithm for quadcopter unmanned aerial vehicles," *Appl. Sci.*, vol. 9, no. 10, 2019, doi: 10.3390/app9102122.

[71] H. Rios, R. Falcon, O. A. Gonzalez, and A. Dzul, "Continuous Sliding-Mode Control Strategies for Quadrotor Robust Tracking: Real-Time Application," *IEEE Trans. Ind. Electron.*, vol. 66, no. 2, pp. 1264–1272, 2019, doi: 10.1109/TIE.2018.2831191.

[72] N. Xuan-Mung, S. K. Hong, N. P. Nguyen, L. N. N. T. Ha, and T. L. Le, "Autonomous quadcopter precision landing onto a heaving platform: New method and experiment," *IEEE Access*, vol. 8, pp. 167192–167202, 2020, doi: 10.1109/ACCESS.2020.3022881.

[73] P. A. Darwito and K. D. Wahyuadnyana, "Performance Examinations of Quadrotor with Sliding Mode Control-Neural Network on Various Trajectory and Conditions," *Math. Model. Eng. Probl.*, vol. 9, no. 3, pp. 707–714, Jun. 2022, doi: 10.18280/mmep.090317.

[74] K. D. Wahyuadnyana and P. A. Darwito, "Parallel Control System PD-SMCNN for Robust Autonomous Mini-Quadcopter," in *2022 International Seminar on Intelligent Technology and Its Applications (ISITIA)*, pp. 244–249, 2022, doi: 10.1109/ISITIA56226.2022.9855371.

[75] O. A. Somefun, K. Akingbade, and F. Dahunsi, "The dilemma of PID tuning," *Annu. Rev. Control*, vol. 52, pp. 65–74, 2021, doi: 10.1016/j.arcontrol.2021.05.002.

[76] R. S. Patil, S. P. Jadhav, and M. D. Patil, "Review of Intelligent and Nature-Inspired Algorithms-Based Methods for Tuning PID Controllers in Industrial Applications," *J. Robot. Control*, vol. 5, no. 2, pp. 336–358, 2024, doi: 10.18196/jrc.v5i2.20850.

[77] T. Hägglund, "The one-third rule for PI controller tuning," *Comput. Chem. Eng.*, vol. 127, pp. 25–30, Aug. 2019, doi: 10.1016/j.compchemeng.2019.03.027.

[78] B. Brahmi, M. H. Laraki, A. Brahmi, M. Saad, and M. H. Rahman, "Improvement of sliding mode controller by using a new adaptive reaching law: Theory and experiment," *ISA Trans.*, vol. 97, pp. 261–268, Feb. 2020, doi: 10.1016/j.isatra.2019.08.010.

[79] N. Xuan-Mung *et al.*, "Novel gain-tuning for sliding mode control of second-order mechanical systems: theory and experiments," *Sci. Rep.*, vol. 13, no. 1, p. 10541, Jun. 2023, doi: 10.1038/s41598-023-37562-7.

[80] S. Chen, D. Li, H. Tian, J. Hou, D. Ning, and Y. Gong, "Experimental study of the effect of internal waves on the rotational hydrodynamics of underwater vehicle," *Int. J. Nav. Archit. Ocean Eng.*, vol. 14, p. 100465, 2022, doi: 10.1016/j.ijnaoe.2022.100465.

[81] L. Cheng *et al.*, "Tuning control parameters of underwater vehicle to minimize the influence of internal solitary waves," *Ocean Eng.*, vol. 310, p. 118681, Oct. 2024, doi: 10.1016/j.oceaneng.2024.118681.